Fractionalized Fermi liquid in a frustrated Kondo lattice model

Johannes S. Hofmann,[1,*] Fakher F. Assaad,[1,†] and Tarun Grover[2,‡]
[1]*Institut für Theoretische Physik und Astrophysik, Universität Würzburg, Am Hubland, D-97074 Würzburg, Germany*
[2]*Department of Physics, University of California at San Diego, La Jolla, California 92093, USA*

(Received 2 August 2018; revised manuscript received 19 February 2019; published 18 July 2019)

We consider Dirac electrons on the honeycomb lattice Kondo coupled to spin-1/2 degrees of freedom on the kagome lattice. The interactions between the spins are chosen along the lines of the Balents-Fisher-Girvin model that is known to host a $\mathbb{Z}_2$ spin-liquid and a ferromagnetic phase. The model is amenable to sign free auxiliary-field quantum Monte Carlo simulations. While in the ferromagnetic phase the Dirac electrons acquire a gap, they remain massless in the $\mathbb{Z}_2$ spin-liquid phase. Since our model has an odd number of spins per unit cell, this phase is a non-Fermi liquid that violates the conventional Luttinger theorem which relates the Fermi surface volume to the particle density in a Fermi liquid. This non-Fermi liquid is a specific realization of the so-called fractionalized Fermi liquid proposed in the context of heavy fermions. We probe the violation of the Luttinger sum rule in this non-Fermi liquid phase via conventional observables such as the spectral function, and also by studying the mutual information between the electrons and the spins.

DOI: 10.1103/PhysRevB.100.035118

I. INTRODUCTION

Electron-electron interactions can localize charge carriers and generate insulating states with local moments [1]. What happens when these local moments (f spins) are Kondo coupled with magnitude J_K to extended Bloch conduction (c) electrons? For a single local moment in a metal, the answer is known: The Kondo coupling is relevant and the f electron is screened by the conduction electrons [2,3]. For a lattice of f electrons, i.e., Kondo lattice systems, the problem is much harder, and the answer is not known in general. However, in the absence of any magnetic ordering, the Lieb-Schultz-Mattis-Hastings-Oshikawa theorem [4–6] puts strong constraints on the possible outcomes. Specifically, in addition to a heavy Fermi liquid phase where the Fermi surface is "large" since it includes the local moments, there exists a distinct possibility where f spins decouple from the conduction electrons at low energies and enter a spin-liquid phase [7,8]. In such a "fractionalized Fermi liquid" phase (henceforth denoted as FL* phase, following Refs. [7,8]), the conduction electron Fermi surface is "small" in that it does not include local moments, and therefore the conventional Luttinger theorem [9] is violated.

From an experimental standpoint, a possible breakdown of Luttinger theorem is relevant to some of the most challenging issues in heavy fermion materials [7,10,11]. There are at least two conceptually different scenarios where this may occur: In materials such as $YbRh_2Si_2$ [12] and $CeCu_{6-x}Au_x$ [13], one observes signatures that indicate that the Fermi surface volume changes abruptly across the transition from a heavy Fermi liquid phase to a magnetically ordered phase characterized by the absence of Kondo screening [14]. A different scenario, which is perhaps more closely related to this paper, is the possibility of a *nonmagnetic phase* which violates Luttinger theorem. Signatures of such a phase were seen in Co- and Ir-doped $YbRh_2Si_2$ [15]. Following Refs. [4,7,8] and as discussed above briefly, in the absence of any other symmetry breaking (e.g., lattice translation) such a nonmagnetic phase is inconsistent with a Fermi liquid ground state if the Kondo screening is not operative and the unit cell contains an odd number of spin-1/2 spins. The local moments in such a phase are then forced to either have a gapless spectrum or topological order [5]. We also note that as discussed in Ref. [16], the above is closely related to the notion of an "orbital selective Mott transition." In addition, there are several other heavy fermionic materials such as CePdAl [17–20], κ-$(ET)_4Hg_{2.89}Br_8$ [21], YbAgGe [22], $YbAl_3C_3$ [23], and Yb_2Pt_2Pb [24] whose phenomenology seems to be poorly understood, and where microscopic considerations suggest that the geometric frustration between local moments plays an important role.

In the next section, we will introduce a generalized Kondo lattice model (KLM) which hosts the aforementioned transition between a conventional phase with electronlike quasiparticles, and an FL* phase with $\mathbb{Z}_2$ topological order. From a technical standpoint, and as discussed in Sec. III, the most salient feature of our model is that it does not suffer from fermion sign problems even in the presence of the Kondo coupling [25]. Our model is realized by Kondo coupling a variant of the Balents-Fisher-Girvin (BFG) model [26–28], first introduced in Ref. [29], to conduction electrons. The BFG model supports a transition from a ferromagnetic phase to a gapped $\mathbb{Z}_2$ spin liquid [Fig. 1(a)]. When this model is weakly coupled to conduction electrons, the spin liquid gives way to an FL* phase where the conduction electrons form a Dirac semimetal, while the local moments continue to form a $\mathbb{Z}_2$ spin liquid [Fig. 1(b)]. Since our unit cell contains two

*johannes.hofmann@physik.uni-wuerzburg.de
†assaad@physik.uni-wuerzburg.de
‡tagrover@ucsd.edu

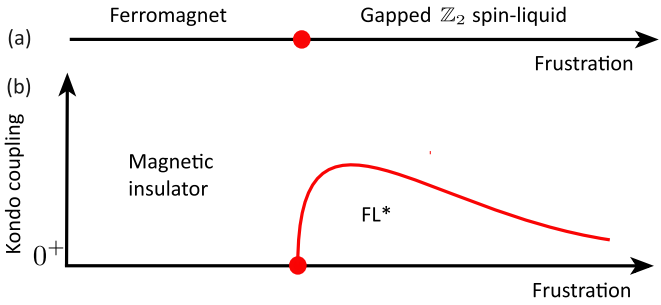

FIG. 1. (a) Schematic phase diagram of the BFG model in the absence of Kondo coupling. (b) Schematic phase diagram of the BFG model in the presence of Kondo coupling. The stability of the FL* phase is set by the gap in the BFG model that scales as $(J^\perp)^2/J^z$ in the strong coupling limit.

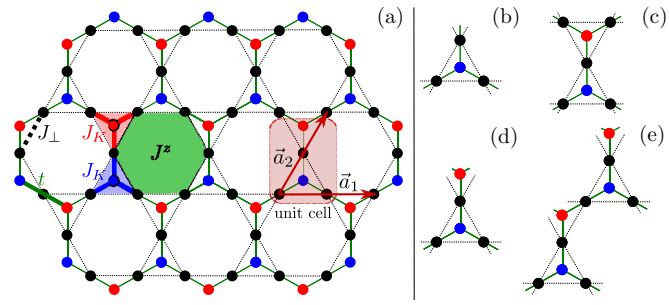

FIG. 2. Left: The model—conduction (c) electrons hop, with matrix element t, between nearest-neighbor sites of the honeycomb lattice denoted by the red and blue circles. The kagome lattice (black) supports impurity spins described by the Balents-Fisher-Girvin model with nearest-neighbor spin-flip $J^\perp$ and interactions on hexagons of strength J^z (green). The two systems are Kondo coupled with strength J_K for each bond in the elemental triangles (thick red and blue bonds). For details, see Eq. (1). Right: Various patches Γ used to extract the Renyi mutual information. Subsets (b) and (c) belong to the triangle sequence, (d) and (e) are built out of unit cells.

c electrons and three f spins, this result stands at odds with the Luttinger sum rule. As the Kondo coupling is increased beyond a threshold, one loses the topological order of the local moments and enters a conventional phase with electronlike quasiparticles. In Sec. IV, we will discuss the numerical results, spectral function of the conduction electrons, and mutual information between the conduction electrons and local moments that allow us to draw the aforementioned conclusion. Finally, in Sec. V, we discuss our results.

II. MODEL AND LIMITING CASES

We investigate the following generalized KLM described by $\hat{H} = \hat{H}_c + \hat{H}_S + \hat{H}_K$ with

$$\hat{H}_c = -t \sum_{\langle \boldsymbol{x},\boldsymbol{y}\rangle,\sigma} \hat{c}^\dagger_{\boldsymbol{x},\sigma}\hat{c}_{\boldsymbol{y},\sigma} + \text{H.c.},$$

$$\hat{H}_S = -J^\perp \sum_{\langle \boldsymbol{i},\boldsymbol{j}\rangle} \left(\hat{S}^{f,+}_{\boldsymbol{i}}\hat{S}^{f,-}_{\boldsymbol{j}} + \text{H.c.}\right) + J^z \sum_{\hexagon} \left(\hat{S}^{f,z}_{\hexagon}\right)^2,$$

$$\hat{H}_K = J_K \sum_{\langle \boldsymbol{x},\boldsymbol{i}\rangle} \left[\hat{S}^{c,z}_{\boldsymbol{x}}\hat{S}^{f,z}_{\boldsymbol{i}} - (-1)^{\boldsymbol{x}}\left(\hat{S}^{c,+}_{\boldsymbol{x}}\hat{S}^{f,-}_{\boldsymbol{i}} + \text{H.c.}\right)\right]. \quad (1)$$

Here, $\hat{c}^\dagger_{\boldsymbol{x},\sigma}$ creates a conduction electron in a Wannier state centered at $\boldsymbol{x}$ with a z component of spin σ, $\boldsymbol{S}^c_{\boldsymbol{x}} = \frac{1}{2}\sum_{s,s'}\hat{c}^\dagger_{\boldsymbol{x},s}\boldsymbol{\sigma}_{s,s'}\hat{c}_{\boldsymbol{x},s'}$ is the spin operator and $\langle \boldsymbol{x},\boldsymbol{y}\rangle$ are the nearest neighbors of a honeycomb lattice. $\boldsymbol{S}^f_{\boldsymbol{i}}$ is a spin-1/2 degree of freedom located on the kagome lattice corresponding to the median of the honeycomb lattice (see Fig. 2). The Hamiltonian $\hat{H}_S$ is a variant of the BFG model (Refs. [26,29]) with nearest-neighbor $\langle \boldsymbol{i},\boldsymbol{j}\rangle$, spin-flip amplitude $J^\perp$, and interaction J^z that minimizes the total z component of the spin on a hexagon: $\hat{S}^{f,z}_{\hexagon} = \sum_{\boldsymbol{i}\in\hexagon}\hat{S}^{f,z}_{\boldsymbol{i}}$. The conduction electrons and the local moments are Kondo coupled, according to $\hat{H}_K$, along nearest-neighbor bonds $\langle \boldsymbol{x},\boldsymbol{i}\rangle$ between the kagome and honeycomb lattices (Fig. 2). The factor $(-1)^{\boldsymbol{x}}$ that takes the value 1 (-1) on the A (B) sublattice of the honeycomb lattice is necessary to avoid the negative sign problem. In particular, it cannot be gauged away since the kagome lattice is not bipartite. Referring back to Fig. 1, J^z plays the role of frustration, and J_K is the Kondo coupling.

Let us consider various limiting cases of the Hamiltonian $\hat{H}$. When $J^\perp \gg J^z, J_K$, the local moments order in an XY-ferromagnetic ground state. Taking into account the $(-1)^{\boldsymbol{x}}$ factor in the Kondo coupling, we see that this term induces an antiferromagnetic in-plane mass term for the conduction electrons. Hence, in this limit one obtains a magnetically ordered insulating phase.

Next, consider $J_K \gg J^\perp \gtrsim J^z, t$. First, let us set all couplings except J_K to zero. Performing the unitary transformation $\hat{c}_{\boldsymbol{x},\downarrow} \to -(-1)^{\boldsymbol{x}}\hat{c}_{\boldsymbol{x},\downarrow}$ maps the Kondo interaction to an antiferromagnetic Heisenberg coupling between the conduction electrons and the local moments. This interaction is not frustrated, and the ground state is AFM ordered with opposite polarizations on the kagome sites and the honeycomb lattice. Undoing the above transformation, the in-plane magnetization of the conduction electrons will be parallel for one honeycomb sublattice and antiparallel for the other, relative to the local moments. Next, turning on a small $J^\perp, J^z$ with $J^\perp \gtrsim J^z$, the local moments will preferably order in the XY plane. Comparing to the limit $J^\perp \gg J^z, J_K$, one finds that the in-plane symmetry-breaking pattern is identical and in the absence of any out-of-plane component, this phase is expected to be adiabatically connected to the aforementioned magnetically ordered insulating phase in the $J^\perp \gg J^z, J_K$ limit. Note that an out-of-plane component will spontaneously break the symmetry $\hat{S}^{f,z}_{\boldsymbol{i}} \to -\hat{S}^{f,z}_{\boldsymbol{i}}$, $\hat{S}^{f,x}_{\boldsymbol{i}} \to \hat{S}^{f,x}_{\boldsymbol{i}}$, $\hat{S}^{f,y}_{\boldsymbol{i}} \to \hat{S}^{f,y}_{\boldsymbol{i}}$ (see Appendix A for a detailed discussion of the symmetries). Due to symmetry breaking and associated stiffness, this phase is also stable to switching on a small hopping t.

Most interesting is the limit $J^z \gg J^\perp \gg J_K$. When only J^z and t are nonzero, the conduction electrons form a Dirac semimetal while the local moments can be described as a classical system with a ground-state degeneracy that scales exponentially with the system size [26]. Allowing a small $J^\perp/J^z \ll 1$ lifts this macroscopic degeneracy and leads to a $\mathbb{Z}_2$ topologically ordered spin liquid of the local moments [26]. Remarkably, as discussed in Refs. [7,8], introducing a small Kondo coupling J_K leaves the state unchanged because perturbatively the Kondo coupling is irrelevant at the

renormalization group (RG) fixed point where conduction electrons form a Dirac semimetal while the local moments are in a gapped $\mathbb{Z}_2$ topologically ordered state. Therefore, at low energies, the local moments decouple from the conduction electrons and one obtains a non-Fermi liquid FL* phase with a "small" Fermi surface which was introduced in Refs. [7,8]. Physically, in this phase the local moments are highly entangled with each other such that the formation of Kondo singlets or the tendency to magnetically order is suppressed.

The phases discussed above, especially the FL* phase, should be contrasted with the conventional heavy Fermi liquid that satisfies the Luttinger sum rule. Since our model has two electrons and three spins per unit cell, the most prominent feature is that this state has a "large" Fermi surface which encloses half of the Brillouin Zone (BZ) whereas the Fermi volume of the aforementioned fractionalized FL* phase vanishes. In the Appendices, we discuss several Ansätze for mean-field approximations of Eq. (1) and find that the nature of the Fermi liquid state strongly depends on symmetries. If particle hole-symmetry (PHS) is imposed in the paramagnetic phase, then one would expect a flat-band pinned at the Fermi level, a generically unstable state [30–38]. A hybridization between c and f electrons necessarily breaks either PHS—with uniform hybridization—or TRS—when the $(-1)^{\boldsymbol{x}}$ phase in the Kondo coupling is carried over to the hybridization. The latter, which should be relevant in magnetic phases especially for large J_K, requires fine-tuning to remain paramagnetic whereas the former can generate a nonmagnetic heavy Fermi liquid. In the range of parameters considered in this paper, we do not find such a phase.

III. METHOD AND OBSERVABLES

We simulate the Hamiltonian in Eq. (1) using the auxiliary field quantum Monte Carlo (QMC) method [39–41]. We follow the strategy outlined in Ref. [25] where it was shown that Hamiltonians of the form $\hat{H}$ do not suffer from the fermion sign problem when $J^{\perp} \geqslant 0$ and the conduction bands are particle-hole symmetric. In this approach, local moments are fermionized, $\boldsymbol{S}_{\boldsymbol{i}}^{f} = \frac{1}{2}\sum_{s,s'} \hat{f}_{\boldsymbol{i},s}^{\dagger} \boldsymbol{\sigma}_{s,s'} \hat{f}_{\boldsymbol{i},s'}$, with the constraint $\sum_s \hat{f}_{\boldsymbol{i},s}^{\dagger}\hat{f}_{\boldsymbol{i},s} = 1$. As in simulations of the generic KLM [42,43], this constraint can be imposed very efficiently since it corresponds to a local conservation law. The details of our implementation are summarized in Appendix B and we have used the ALF package [44] to carry out the simulations. Despite the absence of sign problems, the simulations of this model are challenging. Fermionization leads to a large number of auxiliary fields (33 per unit cell), and the *condition number* on scales corresponding to the ratio of *bandwidth* to the smallest relevant scale (e.g., vison gap in the $\mathbb{Z}_2$ spin-liquid phase) is large. As a consequence, we have used an imaginary time step $\Delta\tau t = 0.01$. The biggest challenge turns out to be large autocorrelation times. We tried to improve this issue by using global moves that mimic vison excitations, as well as by implementing parallel tempering schemes. Nevertheless, these long autocorrelation times remain the limiting factor to access system sizes bigger than those presented here, in particular 3×3 and 6×3 unit cells. For both lattice sizes and the considered periodic boundary conditions, Dirac points are present. However, only the 6×3 allows us to satisfy $\hat{S}^{f,z}_{\hexagon} = 0$ for all hexagons. Note that mass gaps generically decrease with system size in this setup [45,46], which is confirmed by the comparison of spectra on 3×3 and 6×3 lattices, such that gapless Dirac cones constitute strong evidence for the decoupling of the $\mathbb{Z}_2$ spin liquid and the Dirac fermions.

We compute spin-spin correlations $S_{\mathrm{AFM}} = 1/L \sum_{\boldsymbol{IJ}} \langle \hat{S}^{x}_{\boldsymbol{I}} \hat{S}^{x}_{\boldsymbol{J}} + \hat{S}^{y}_{\boldsymbol{I}} \hat{S}^{y}_{\boldsymbol{J}} \rangle$ where the net spin per unit cell $\boldsymbol{I}$, $\hat{\boldsymbol{S}}_{\boldsymbol{I}} = \sum_{\boldsymbol{i}\in\boldsymbol{I}} \hat{\boldsymbol{S}}^{f}_{\boldsymbol{i}} + \sum_{\boldsymbol{x}\in\boldsymbol{I}} (-1)^{\boldsymbol{x}} \hat{\boldsymbol{S}}^{c}_{\boldsymbol{x}}$, captures the aforementioned ferromagnetic-antiferromagnetic order of the f spins and conduction electrons. The spectral function of the conduction electrons $A_c(\boldsymbol{k},\omega) = -\frac{1}{\pi}\,\mathrm{Im}\, G_c^{\mathrm{ret}}(\boldsymbol{k},\omega)$ can be extracted from the imaginary time-resolved Green's function $G_c(\boldsymbol{k},\tau) = \sum_{\alpha,\sigma} \langle \hat{c}^{\dagger}_{\boldsymbol{k},\alpha,\sigma}(\tau) \hat{c}_{\boldsymbol{k},\alpha,\sigma}(0) \rangle$ using the MaxEnt method [47,48]. Here α is the orbital index. The auxiliary field QMC method also allows us to study the entanglement properties of fermionic models [49–54]. In particular, as shown in Refs. [50,51], the second Renyi entropy S_2 can be computed from the knowledge of Green's-functions G_A, restricted to subsystem A, for two independent Monte Carlo samples. An alternative approach exploits the replica trick, e.g., for fermionic [55–58], bosonic [29], and spin systems [59,60]. For a given subsystem of conduction electrons Γ_c and of spins Γ_f, the Renyi mutual information between Γ_c and Γ_f is $I_2(\Gamma_c,\Gamma_f) \equiv -S_2(\Gamma_c \cup \Gamma_f) + S_2(\Gamma_c) + S_2(\Gamma_f)$. We use the two sequences for Γ as shown in Figs. 2(b), 2(c) 2(d), and 2(e). In the calculation of the Renyi mutual information, we restore the C_3 lattice symmetry by averaging over rotationally equivalent Γs.

IV. RESULTS

From here on, we fix $J^{\perp} = t$ and use $t = 1$ as the unit of energy. The BFG model shows a transition from the ferromagnetic state to the $\mathbb{Z}_2$ spin liquid at $J_c^z \simeq 7.07$ [29]. Alongside with spin excitations, the $\mathbb{Z}_2$ spin liquid hosts vison excitations. Recent simulations of the dynamics of the BFG model [61] estimate the spin and vison gaps at $J^z = 8.\overline{3}$ to $\Delta_s \simeq 7.12$ and $\Delta_v \simeq 0.2$. We expect that the vison gap remains nonzero at the transition and that the spin gap scales as $(J^z - J_c^z)^{\nu z}$ with dynamical critical exponent $z = 1$ and $\nu \simeq 0.67$, which correspond to the exponents of the 3D XY* model [27,62,63].

Figure 3 shows a scan at $J^z = 7.5$ as a function of J_K. We have set the temperature to $\beta = 12$. From the above discussion, this choice of temperature places us well below the spin gap and allows us to resolve the vison gap. As apparent in Fig. 3(c), the single particle spectral function at the Dirac point remains gapless. As a function of J_K it looses spectral weight and a full gap opens sightly before $J_K = 1.5$. At this energy scale, the spin-spin correlations S_{AFM} show a marked upturn [see Fig. 3(a)]. In the presence of long-ranged magnetic order S_{AFM} scales as the volume of the system. Comparison between the 3×3 and 3×6 lattices shows that S_{AFM} grows as a function of system size beyond $J_K = 1.5$.

Small values of J_K are associated with small energy scales which may be difficult to resolve on our finite sized systems at finite temperatures. To confirm the above result, we present a scan at fixed $J_K = 1$ and vary J^z in Fig. 4. Upon analysis

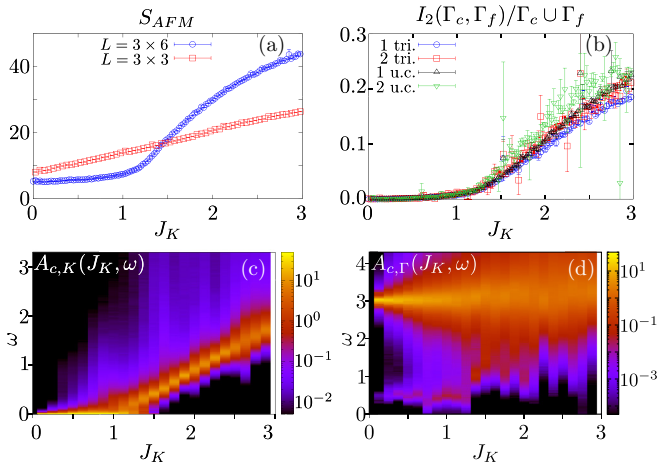

FIG. 3. We consider lattices $L = 3 \times 3$ and $L = 3 \times 6$ unit cells at an inverse temperature $\beta = 12$ and at $J^z = 7.5$ (a) Spin-spin correlations S_{AFM} (see text), (b) Renyi mutual informations $I_2(\Gamma_c, \Gamma_f)$ per site of the patch $\Gamma_c \cup \Gamma_f$ for $L = 3 \times 6$. Here we consider the patches listed in Figs. 2(b)–2(e). (c) Conduction electron spectral function at the Dirac point $\boldsymbol{K}$ for the 3×6 lattice. (d) Same as (c), but at the Γ-point. The imaginary time data from which panels (c) and (d) stem are presented in Appendix C.

of Figs. 4(a) and 4(c), one concludes that the magnetic order and the single-particle gap track each other. In particular, the single-particle gap closes in the $\mathbb{Z}_2$ spin-liquid phase.

Signatures of the $\mathbb{Z}_2$ spin-liquid phase can be picked up in the spectrum of the conduction electrons. In Figs. 3(d) and 4(d), we plot the single-particle spectral function at the Γ point. In the FL* phase one notices spectral weight at low energies that we interpret as a signature of the vison. In particular, since the vison carries no $\mathbb{Z}_2$ charge, it will

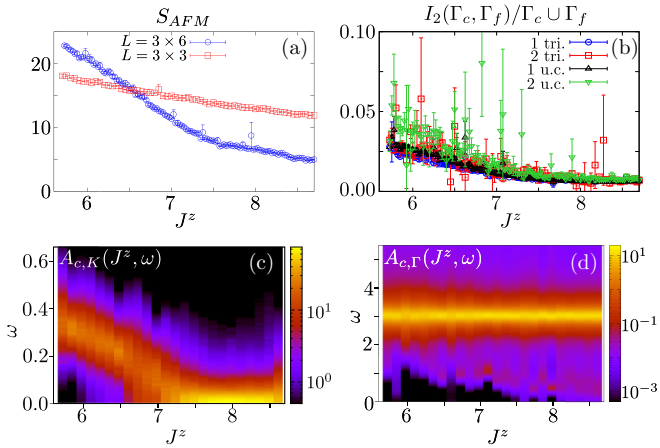

FIG. 4. We consider lattices $L = 3 \times 3$ and $L = 3 \times 6$ unit cells at an inverse temperature $\beta = 12$ and at $J_K = 1$ (a) Spin-spin correlations S_{AFM} (see text), (b) Renyi mutual information $I_2(\Gamma_c, \Gamma_f)$ per site of the patch $\Gamma_c \cup \Gamma_f$ for $L = 3 \times 6$. Here we consider the patches listed in Figs. 2(b)–2(e). (c) Conduction electron spectral function at the Dirac point $\boldsymbol{K}$ for the 3×6 lattice. (d) same as (c), but at the Γ-point. The imaginary time data from which panels (c) and (d) stem are presented in the Appendices.

generically couple to conduction electrons and show up in the spectral function.

It is interesting to consider other measures for Kondo screening. The Renyi mutual information I_2 between the c electrons and the f spins introduced above provides one such measure [64]. It is important to note that this quantity is both IR and UV sensitive since we are considering mutual information between two Hilbert spaces that overlap in real space. Despite the decoupling of conduction electrons and local moments at low energies in the FL* phase, one therefore doesn't except that the mutual information will be exactly zero in this phase. It vanishes only at the RG fixed point corresponding to $J_K = 0$, where these two Hilbert spaces completely decouple. In the opposite limit when the c electrons and f spins are maximally entangled, the Renyi mutual information will attain its maximum possible value of $4\log(2)/5$ per site (recall that the unit cell of our model contains three f spins and two c electrons). In the magnetically ordered phase, one expects that the Renyi mutual information will not be close to this maximum due to the entanglement between the local moments themselves. From Figs. 3(b) and 4(c), we see that the QMC data is consistent with this expectation. The most notable feature is that the Renyi mutual information per site is an order of magnitude smaller in the FL* phase compared to the magnetically ordered phase. Such a dramatic drop is not seen in the generic Kondo lattice [64]. Furthermore, even on a limited size lattices such as ours, one can already see signatures of the transition from the magnetically ordered phase to the FL* phase as evidenced by the change of slope in the coefficient of the Renyi mutual information at the transition.

V. CONCLUSION AND DISCUSSION

In this paper, we introduced a model amenable to negative sign free Monte Carlo simulations that can host a fractionalized Fermi liquid (FL*) phase. The most prominent feature of this phase is a violation of the Luttinger theorem due to the onset of topological order. This proof of principle calculation paves the way to many other investigations. We have considered a model where the fractionalization inherent to topological order is "emergent," i.e., the lattice model is written in terms of spins. A different, and possibly numerically more tractable approach, would be to simulate directly a theory of spinons coupled to $\mathbb{Z}_2$ gauge fields following Refs. [65–67] and where spinons are also Kondo coupled to conduction electrons. Such an approach might be particularly useful for studying the quantum phase transition between the FL* phase and the magnetically ordered phase. A field theory description of this transition was provided in Ref. [63], where it was found that the Kondo coupling is irrelevant at the critical point due to the large anomalous exponent of the spins, and therefore one expects that the conduction electrons have a well-defined electronlike quasiparticle even at the critical point, while the local moments will inherit the critical exponents of the 3D XY* transition [27,62].

It might also be interesting to explore the possibility of obtaining nontrivial symmetry-protected topological phases in frustrated Kondo models along the lines of Ref. [68] where it was shown that under certain conditions, one can obtain

symmetric states without any topological order even when the unit cell contains an odd number of spins but the magnetic unit cell has an integral number of spins.

Another avenue to explore would be the universal subleading contribution of the Renyi entanglement entropy for a spatial bipartition. In the FL* phase, one expects that this contribution is given as $\gamma = \gamma_{\text{topo}} + \gamma_{\text{Dirac}}$, where $\gamma_{\text{topo}} = \log(2)$ is the topological entanglement entropy corresponding to the topological order of the local moments, while γ_{Dirac} is the shape-dependent universal contribution from the Dirac conduction electrons [69,70]. Similarly, at the transition, owing to the aforementioned irrelevance of the Kondo coupling, one expects that $\gamma = \gamma_{\text{topo}} + \gamma_{\text{Dirac}} + \gamma_{\text{3D XY}}$ where $\gamma_{\text{3D XY}}$ is the universal shape-dependent entanglement contribution at the 3D XY transition [69].

Finally, as mentioned in the introduction, the violation of the Luttinger sum rule is central to several questions in heavy fermion materials as well as frustrated Kondo lattice systems. Our approach opens a potential window to quantitatively explore these and related questions as well.

ACKNOWLEDGMENTS

The authors thank T. Sato and F. Parisen-Toldin for stimulating discussions and S. Sachdev and A. Vishwanath for comments on the draft. J.S.H. and F.F.A. are supported by the German Research Foundation (DFG), under DFG-SFB No. 1170 ToCoTronics (Project No. C01). T.G. is supported by the National Science Foundation under Grant No. DMR-1752417 and as an Alfred P. Sloan research fellow. The authors gratefully acknowledge the Gauss Centre for Supercomputing e.V. (www.gauss-centre.eu) for funding this project by providing computing time on the GCS Supercomputer SuperMUC at Leibniz Supercomputing Centre (LRZ, www.lrz.de). We also acknowledge the Bavaria California Technology Center (BaCaTeC) for travel support.

APPENDIX A: SYMMETRIES AND HEAVY FERMI LIQUIDS

In this section, we consider nonmagnetic mean-field solutions such as the Kondo insulator and the heavy Fermi liquid phase realized in conventional Kondo systems. To this end, it is convenient to introduce the following two operators: $\hat{\Delta}^0_{\boldsymbol{x},\boldsymbol{i}} = \sum_s \hat{c}^\dagger_{\boldsymbol{x},s}\hat{f}_{\boldsymbol{i},s} + \text{H.c.}$ and $\hat{\Delta}^z_{\boldsymbol{x},\boldsymbol{i}} = \hat{c}^\dagger_{\boldsymbol{x},\uparrow}\hat{f}_{\boldsymbol{i},\uparrow} - (-1)^{\boldsymbol{x}}\hat{c}^\dagger_{\boldsymbol{x},\downarrow}\hat{f}_{\boldsymbol{i},\downarrow} + \text{H.c.}$ so the Kondo coupling of Eq. (1) of the main text can be written as $\hat{H}_K = -\frac{J_K}{4}\sum_{\langle \boldsymbol{x},\boldsymbol{i}\rangle}(\hat{\Delta}^z_{\boldsymbol{x},\boldsymbol{i}})^2$. Whereas the former usually generates the Kondo insulator in conventional Kondo systems at half filling and also the heavy Fermi liquid at finite doping, the later is more natural in the model defined by Eq. (1) of the main text due to the sign structure of the Kondo coupling. In the following, we first describe the symmetries of the system and then discuss their implications for nonmagnetic mean-field approximations.

Our model, Eq. (1) of the main text, has several continuous and discrete symmetries. Among continuous symmetries, the number of conduction electrons is conserved, and so is the projection of the total spin along the z direction, i.e., $\sum_{\boldsymbol{x}} \hat{S}^{c,z}_{\boldsymbol{x}} + \sum_{\boldsymbol{i}} \hat{S}^{f,z}_{\boldsymbol{i}}$.

TABLE I. Table of independent particle-hole symmetries. See text for the notation.

U	σ^x	σ^z	σ^0	σ^0
α	−	−	+	−
β_x	−	+	−	−
β_y	+	+	+	−
β_z	+	−	−	−

The model also exhibits several unitary and antiunitary particle-hole symmetries which we list in Table I. They are implemented by a matrix U via $\hat{c}^\dagger_{\boldsymbol{x},s} \to (-1)^{\boldsymbol{x}} U_{s,s'}\hat{c}_{\boldsymbol{x},s'}$ and $\hat{f}^\dagger_{\boldsymbol{i},s} \to U_{s,s'}\hat{f}_{\boldsymbol{i},s'}$ together with the sign α distinguishing between unitary and antiunitary transformations: $\sqrt{-1} \to \alpha\sqrt{-1}$. We list their action on the spin operators by the signs $\boldsymbol{\beta} = (\beta_x, \beta_y, \beta_z)$ with $\hat{S}^{c,l}_{\boldsymbol{x}} \to \beta_l \hat{S}^{c,l}_{\boldsymbol{x}}$ as well as $\hat{S}^{f,l}_{\boldsymbol{i}} \to \beta_l \hat{S}^{c,l}_{\boldsymbol{i}}$.

One can also combine the particle-hole symmetries in Table I to define two different antiunitary time-reversal symmetries. The first one, TR_1, is defined via $\hat{c}^\dagger_{\boldsymbol{x},s} \to i\sigma^y_{s,s'}\hat{c}^\dagger_{\boldsymbol{x},s'}$ and $\hat{f}^\dagger_{\boldsymbol{i},s} \to i\sigma^y_{s,s'}\hat{f}^\dagger_{\boldsymbol{i},s'}$ along with $\sqrt{-1} \to -\sqrt{-1}$. This transformation flips all three components of the spin operators $\hat{\boldsymbol{S}}^c_{\boldsymbol{x}} \to -\hat{\boldsymbol{S}}^c_{\boldsymbol{x}}$ as well as $\hat{\boldsymbol{S}}^f_{\boldsymbol{i}} \to -\hat{\boldsymbol{S}}^f_{\boldsymbol{i}}$. The second one, TR_2, replaces $i\sigma^y$ by σ^x so only the z component of the spin operators gets reversed.

At the level of free fermion band-structure, the particle-hole symmetries listed above lead to flat bands. In particular, either of the symmetries $(U, \alpha) = (\sigma^0, -)$ and $(U, \alpha) = (\sigma^z, -)$ guarantee that there is a flat band. This is because these transformations do not mix up and down spin components, which leads to an odd number (= five) of bands for each spin sector. Furthermore, the antiunitary nature of the symmetry implies that $c(k) \to c^\dagger(k)$. Thus there always exists a flat band at zero energy in each spin sector. Such a flat band will generically be unstable to interactions, e.g., according to Table I, a magnetically ordered state in the z direction will break both of these particle-hole symmetries.

A natural mean-field approximation uses the hybridization term $\hat{\Delta}^z = \sum_{\langle \boldsymbol{x},\boldsymbol{i}\rangle} \hat{\Delta}^z_{\boldsymbol{x},\boldsymbol{i}}$ which preserves the PHS listed as $(\sigma^x, -)$ in Table I, but breaks $(\sigma^z, -)$, $(\sigma^0, +)$ and $(\sigma^0, -)$, as well as TR_1 and TR_2. The mean-field Hamiltonian $\hat{H}_c + \hat{\Delta}^z$ still has a spin-degenerate flat band at the chemical potential such that a magnetization in the z direction, which respects the S^z-spin-rotation symmetry, should be included as well. This is a magnetically ordered state and numerically we find no evidence for a finite magnetization in the z direction.

Let us next consider mean-field solutions based on symmetry arguments. As discussed before, to obtain dispersive bands one would need to break at least some symmetries. One option is the uniform hybridization, $\sum_{\langle \boldsymbol{x},\boldsymbol{i}\rangle} \hat{\Delta}^0_{\boldsymbol{x},\boldsymbol{i}}$, that preserves the time-reversal symmetries TR_1 and TR_2, but breaks all particle-hole symmetries. As a consequence, one should also allow direct f-electron hopping terms given by $\sum_{\langle \boldsymbol{i},\boldsymbol{j}\rangle,s} \hat{f}^\dagger_{\boldsymbol{i},s}\hat{f}_{\boldsymbol{j},s} + \text{H.c.}$ The mean-field Hamiltonian for such a heavy Fermi Liquid is then given as

$$\hat{H}_{\text{hFL}} = \hat{H}_c + \Delta \sum_{\langle \boldsymbol{x},\boldsymbol{i}\rangle} \hat{\Delta}^0_{\boldsymbol{x},\boldsymbol{i}} + t' \sum_{\langle \boldsymbol{i},\boldsymbol{j}\rangle,s} \hat{f}^\dagger_{\boldsymbol{i},s}\hat{f}_{\boldsymbol{j},s} + \text{H.c.} \qquad \text{(A1)}$$

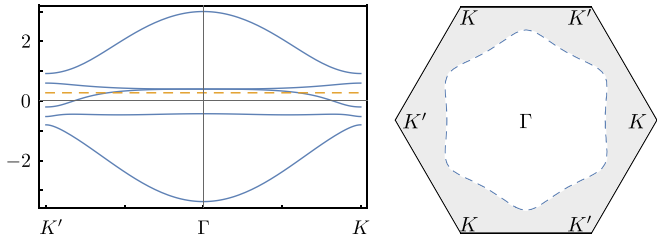

FIG. 5. Cut of the spectrum from K' to K with the Fermi energy marked by the dashed, orange line constraint to the half-filled case and Fermi surface (blue, dashed) of a heavy Fermi Liquid state with $\Delta = 0.4$ and $t' = 0.2$. The shaded area marks the occupied part of the BZ.

The resulting band structure is depicted in Fig. 5 for $\Delta = 0.4$ and $t' = 0.2$, where the left-hand side shows a cut from K' to Γ to K. We clearly recognize a dispersive band in the middle of the spectrum replacing the aforementioned flat band at zero energy. Each band is spin degenerate which enhances the S_z symmetry to a full $SU(2)$ and consequently, the state is paramagnetic. The right-hand side of the figure shows the Fermi surface (blue, dashed) where we have kept the electron density fixed at half-filling. Consistent with Oshikawa's argument [4], one finds that the Fermi surface is large, and occupies half of the Brillouin zone which is depicted by the shaded area in Fig. 5. The effective chemical potential required for half-filling is marked by the dashed orange line in the left-hand side of Fig. 5.

To summarize, the natural mean-field decoupling of Eq. (1) of the main text leads to a magnetic phase and a symmetry-based approach generates a heavy Fermi liquid that we do not find numerically in the investigated range of parameters.

APPENDIX B: DETAILS OF THE METHOD

Let us first write down the fermionized Hamiltonian that is simulated, $\hat{H}_{\mathrm{qmc}}$, and then show its equivalence to Eq. (1) of the main text:

$$\hat{H}_{\mathrm{qmc}} = -t \sum_{\langle \boldsymbol{x},\boldsymbol{y}\rangle,\sigma} \hat{\tilde{c}}^{\dagger}_{\boldsymbol{x},\sigma}\hat{\tilde{c}}_{\boldsymbol{y},\sigma} + \mathrm{H.c.} - \frac{J^{\perp}}{4}\sum_{\langle \boldsymbol{i},\boldsymbol{j}\rangle}\left[2\left(\sum_{\sigma}\hat{\tilde{f}}^{\dagger}_{\boldsymbol{i},\sigma}\hat{\tilde{f}}_{\boldsymbol{j},\sigma} + \mathrm{H.c.}\right)^2 + \left(n^{\tilde{f}}_{\boldsymbol{i}} + n^{\tilde{f}}_{\boldsymbol{j}} - 1\right)^2\right]$$
$$- \frac{J^{z}}{4}\sum_{\hexagon}\sum_{\boldsymbol{i}\in\hexagon<\boldsymbol{j}\in\hexagon}\left(n^{\tilde{f}}_{\boldsymbol{i}} - n^{\tilde{f}}_{\boldsymbol{j}}\right)^2 - \frac{J_K}{4}\sum_{\langle \boldsymbol{i},\boldsymbol{x}\rangle}\left(\sum_{\sigma}\hat{\tilde{f}}^{\dagger}_{\boldsymbol{i},\sigma}\hat{\tilde{c}}_{\boldsymbol{x},\sigma} + \mathrm{H.c.}\right)^2, \tag{B1}$$

with $(\hat{\tilde{c}}^{\dagger}_{\boldsymbol{x},\uparrow}, \hat{\tilde{c}}^{\dagger}_{\boldsymbol{x},\downarrow}) = (\hat{c}^{\dagger}_{\boldsymbol{x},\uparrow}, (-1)^{\boldsymbol{x}}\hat{c}_{\boldsymbol{x},\downarrow})$ and $(\hat{\tilde{f}}^{\dagger}_{\boldsymbol{i},\uparrow}, \hat{\tilde{f}}^{\dagger}_{\boldsymbol{i},\downarrow}) = (\hat{f}^{\dagger}_{\boldsymbol{i},\uparrow}, \hat{f}_{\boldsymbol{i},\downarrow})$. The Hamiltonian above is identical to Eq. (1) of the main text up to the following five terms in $\hat{H}_{\mathrm{qmc}} - \hat{H}$. The first term $+(J^{\perp} + 4J^{z})\sum_{\boldsymbol{i}}(n^{f}_{\boldsymbol{i}} - 1)^2$ is the well-known repulsive Hubbard interaction that suppresses charge fluctuations. The local parity of the f electrons $(n^{f}_{\boldsymbol{i}} - 1)^2$ commutes with the Hamiltonian as the relevant terms $+J^{\perp}\sum_{\langle \boldsymbol{i},\boldsymbol{j}\rangle}\hat{f}^{\dagger}_{\boldsymbol{i},\uparrow}\hat{f}^{\dagger}_{\boldsymbol{i},\downarrow}\hat{f}_{\boldsymbol{j},\downarrow}\hat{f}_{\boldsymbol{j},\uparrow} + \mathrm{H.c.}$ and $+\frac{J_K}{2}\sum_{\langle \boldsymbol{i},\boldsymbol{x}\rangle}(-1)^{\boldsymbol{x}}\hat{f}^{\dagger}_{\boldsymbol{i},\uparrow}\hat{f}^{\dagger}_{\boldsymbol{i},\downarrow}\hat{c}_{\boldsymbol{x},\downarrow}\hat{c}_{\boldsymbol{x},\uparrow} + \mathrm{H.c.}$ modify the local occupation by 2. Hence the Hubbard interaction projects onto the sector with singly occupied f-electron sites exponentially fast and the relevant scale is set by $\beta(J^{\perp} + 4J^{z})$. In this subspace, all other contributions of $+\frac{J^{\perp}}{2}\sum_{\langle \boldsymbol{i},\boldsymbol{j}\rangle}(n^{f}_{\boldsymbol{i}} - 1)(n^{f}_{\boldsymbol{j}} - 1)$ and $+\frac{J_K}{4}\sum_{\langle \boldsymbol{i},\boldsymbol{x}\rangle}(n^{f}_{\boldsymbol{i}} - 1)(n^{c}_{\boldsymbol{x}} - 1)$ vanish such that $\hat{H}_{\mathrm{qmc}}|_{(n^{f}_{\boldsymbol{i}}-1)^2=0} = \hat{H}$. The interested reader is referred to the Supplemental Material, i.e., Eq. (9) of Ref. [25].

The efficient projection due to the repulsive Hubbard interaction, however, also introduces a challenge for the numerical stability of the algorithm. Here we have to control the various scales of $A_j = \prod_{i=0}^{j} B_i$ where B_i is the product of all exponentiated operators on the ith time slice. Apparently, this model generated eigenvalues in A_j which exceeded the range of double precision which is of order $10^{\pm 308}$. To overcome this issue, we implemented the following stabilization scheme. Assume that we already have a QR decomposition of $A_{j-1} = Q_{j-1}e^{\lambda_{j-1}}R_{j-1}$ where Q_{j-1} is the orthogonal part, $e^{\lambda_{j-1}}$ is diagonal and separates the main scales, and R_{j-1} contains the mixing of them. To generate $A_j = B_j A_{j-1}$ we perform the following steps:

(1) Calculate $M_j = B_j Q_{j-1}$.

(2) Use the permutation P_j to sort the columns of $M_j = \tilde{M}_j P_j$ according to the column norm of $M_j e^{\lambda_{j-1}}$. Permute λ_{j-1} and R_{j-1} with P_j^{-1} to correct this manipulation.

(3) Perform a QR decomposition of $M_j = Q_j \tilde{R}_j$ without pivoting.

(4) Extract the scales of $\tilde{R}$ as $(D_j)_n = |(\tilde{R}_j)_{nn}|$.

(5) Determine the new scales $\lambda_j = \log(D_j) + \lambda_{j-1}$.

(6) Calculate $R_j = D_j^{-1}e^{-\lambda_{j-1}}\tilde{R}_j e^{\lambda_{j-1}}R_{j-1}$.

This scheme keeps all the advantages of QR decomposition with pivoting to handle exponentially large and small scales of A_j which is paramount to a stable Blankenbecler Scalapino Sugar (BSS) algorithm, even when double precision suffices. Here, we did not store the scales as Ds but rather as $e^{\lambda_{j-1}}$ to handle numbers much larger than $10^{\pm 308}$.

APPENDIX C: TIME-DISPLACED GREEN'S FUNCTION

Here we provide the imaginary time displaced Green's functions of conduction electrons, $G_c(\boldsymbol{k},\tau) = \sum_{\alpha,\sigma}\langle \hat{c}^{\dagger}_{\boldsymbol{k},\alpha,\sigma}(\tau)\hat{c}_{\boldsymbol{k},\alpha,\sigma}(0)\rangle$ where α is the orbital and σ the spin index. The dynamical data presented in the main text, is obtained by solving

$$G_c(\boldsymbol{k},\tau) = \frac{1}{\pi}\int d\omega \frac{e^{-\tau\omega}}{1 + e^{-\beta\omega}}A_c(\boldsymbol{k},\omega) \tag{C1}$$

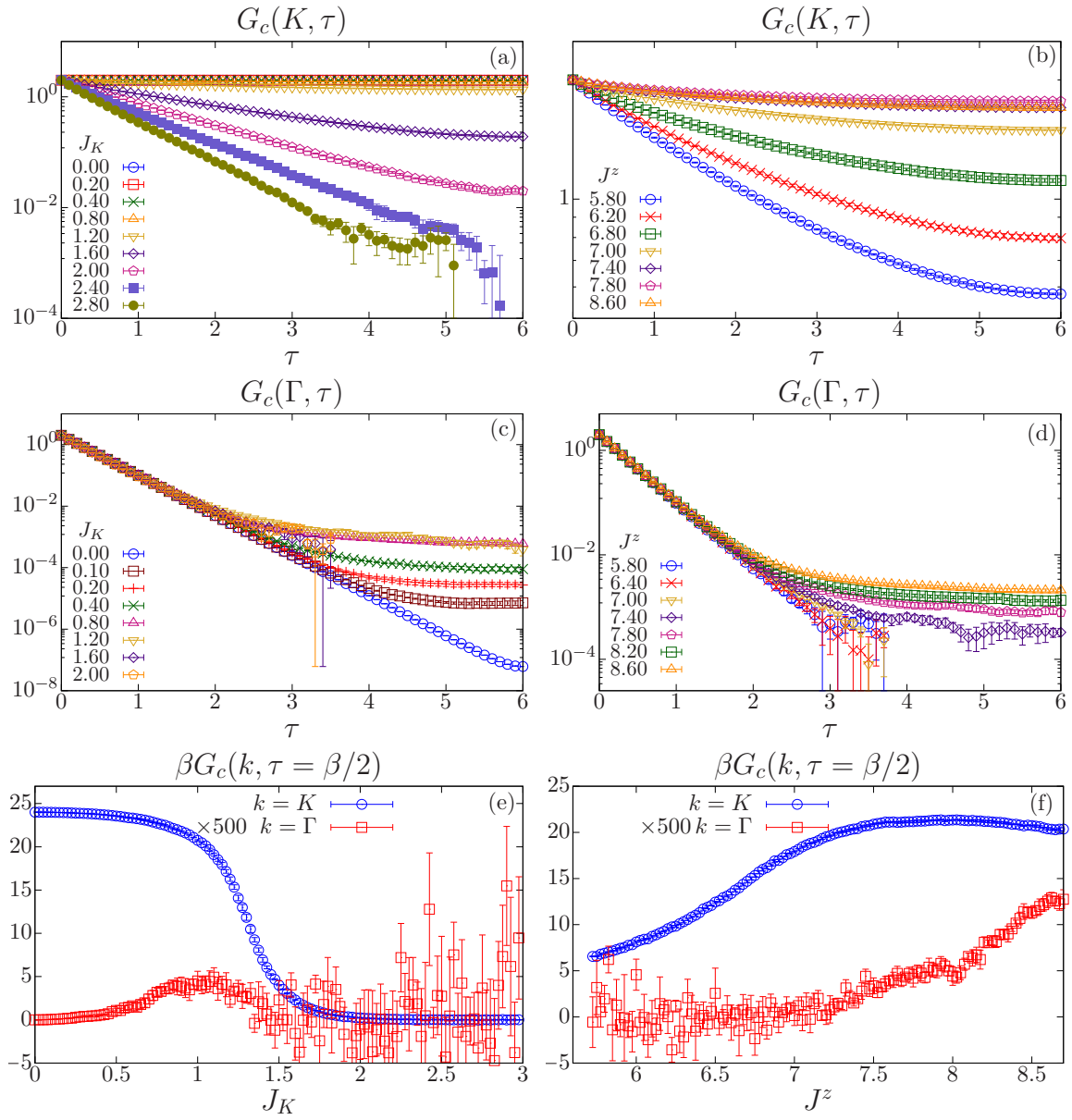

FIG. 6. The simulations were performed on the $L = 3 \times 6$ lattice at an inverse temperature of $\beta = 12$. Left panels corresponds to the J_K scan at $J^z = 7.5$ and the right to the J^z scan at $J_K = 1.0$. For large J_K or small J^z, we restricted the time domain in (c) and (d) to $\tau < 3.5$ and $\tau < 3.75$, respectively, since beyond this scale, the data becomes very noisy.

for $A_c(\boldsymbol{k}, \omega)$ using the stochastic maximum entropy method [47,48]. The features present in the dynamical data can clearly be detected in the imaginary time data which we report in this section. In Fig. 6, the left-hand side panels presents the J_K scan at a fixed $J^z = 7.5$ whereas on the right-hand side we show the J^z scan at constant $J_K = 1.0$.

Figures 6(a) and 6(b) depict the Green's function at the Dirac points. In both cases, the gapless mode is clearly visible in the FL* phase since $G_c(\boldsymbol{K}, \tau)$ shows a plateau at *large* imaginary times. This height of the plateau corresponds to the quasiparticle residue.

Figures 6(c) and 6(d) present the equivalent data but at the Γ point. In the FL* phase, we see a clear feature with small intensity at *large* values of τ. It is this feature in the imaginary time Green's function that generates the low-energy spectral weight in Figs. 3(d) and 4(d) of the main text in the FL* phase. As mentioned in the paper, we interpret this feature as a signature of the vison excitation.

Another possible analysis stems from the identity

$$\lim_{\beta\to\infty} \beta G_c(\boldsymbol{k}, \tau = \beta/2) = A_c(\boldsymbol{k}, \omega = 0), \tag{C2}$$

which holds provided that $A_c(\boldsymbol{k}, \omega)$ is a smooth function. At finite values of β, $\beta G_c(\boldsymbol{k}, \tau = \beta/2)$ will provide an estimate of the spectral weight in an energy window around $\omega = 0$ of width set by $1/\beta$. Panels (e) and (f) of Fig. 6 plot this quantity both at the Γ and Dirac points. Overall, these panels again confirm that in the FL* phase we observe low-energy excitations with small intensity at the Γ point and low-energy excitations with large spectral weight at the Dirac point. Note that in

panel (e) of Fig. 6, corresponding to the J_K scan, the intensity of the feature at the Γ point first grows and then decreases since both at $J_K = 0$, where the spin and conduction electrons decouple and the conduction electrons form a Dirac spectrum, and at $J_K \gg 1$, where in the magnetic insulating phase, no low-lying single particle weight is expected at the Γ point.

[1] M. Imada, A. Fujimori, and Y. Tokura, Rev. Mod. Phys. **70**, 1039 (1998).
[2] P. W. Anderson, J. Phys. C: Solid State Phys. **3**, 2436 (1970).
[3] A. C. Hewson, *The Kondo Problem to Heavy Fermions*, Cambridge Studies in Magnetism (Cambridge University Press, Cambridge, 1997).
[4] M. Oshikawa, Phys. Rev. Lett. **84**, 3370 (2000).
[5] M. B. Hastings, Phys. Rev. B **69**, 104431 (2004).
[6] E. Lieb, T. Schultz, and D. Mattis, Ann. Phys. **16**, 407 (1961).
[7] T. Senthil, S. Sachdev, and M. Vojta, Phys. Rev. Lett. **90**, 216403 (2003).
[8] T. Senthil, M. Vojta, and S. Sachdev, Phys. Rev. B **69**, 035111 (2004).
[9] J. M. Luttinger, Phys. Rev. **119**, 1153 (1960).
[10] P. Coleman, C. Pépin, Q. Si, and R. Ramazashvili, J. Phys.: Condens. Matter **13**, R723 (2001).
[11] Q. Si, S. Rabello, K. Ingersent, and J. Smith, Nature **413**, 804 (2001).
[12] S. Paschen, T. Lühmann, S. Wirth, P. Gegenwart, O. Trovarelli, C. Geibel, F. Steglich, P. Coleman, and Q. Si, Nature **432**, 881 (2004).
[13] M. Klein, A. Nuber, F. Reinert, J. Kroha, O. Stockert, and H. v. Löhneysen, Phys. Rev. Lett. **101**, 266404 (2008).
[14] S. J. Yamamoto and Q. Si, Phys. Rev. Lett. **99**, 016401 (2007).
[15] S. Friedemann, T. Westerkamp, M. Brando, N. Oeschler, S. Wirth, P. Gegenwart, C. Krellner, C. Geibel, and F. Steglich, Nat. Phys. **5**, 465 (2009).
[16] M. Vojta, J. Low Temp. Phys. **161**, 203 (2010).
[17] A. Dönni, G. Ehlers, H. Maletta, P. Fischer, H. Kitazawa, and M. Zolliker, J. Phys.: Condens. Matter **8**, 11213 (1996).
[18] T. Goto, S. Hane, K. Umeo, T. Takabatake, and Y. Isikawa, J. Phys. Chem. Solids **63**, 1159 (2002), proceedings of the 8th ISSP International Symposium.
[19] A. Oyamada, S. Maegawa, M. Nishiyama, H. Kitazawa, and Y. Isikawa, Phys. Rev. B **77**, 064432 (2008).
[20] A. Sakai, S. Lucas, P. Gegenwart, O. Stockert, H. v. Löhneysen, and V. Fritsch, Phys. Rev. B **94**, 220405(R) (2016).
[21] H. Oike, Y. Suzuki, H. Taniguchi, K. Miyagawa, and K. Kanoda, arXiv:1602.08950 [cond-mat.str-el] .
[22] M. S. Kim, M. C. Bennett, and M. C. Aronson, Phys. Rev. B **77**, 144425 (2008).
[23] K. Sengupta, M. K. Forthaus, H. Kubo, K. Katoh, K. Umeo, T. Takabatake, and M. M. Abd-Elmeguid, Phys. Rev. B **81**, 125129 (2010).
[24] Y. Kato, M. Kosaka, H. Nowatari, Y. Saiga, A. Yamada, T. Kobiyama, S. Katano, K. Ohoyama, H. S. Suzuki, N. Aso, and K. Iwasa, J. Phys. Soc. Jpn. **77**, 053701 (2008).
[25] T. Sato, F. F. Assaad, and T. Grover, Phys. Rev. Lett. **120**, 107201 (2018).
[26] L. Balents, M. P. A. Fisher, and S. M. Girvin, Phys. Rev. B **65**, 224412 (2002).
[27] S. V. Isakov, Y. B. Kim, and A. Paramekanti, Phys. Rev. Lett. **97**, 207204 (2006).
[28] S. V. Isakov, A. Paramekanti, and Y. B. Kim, Phys. Rev. B **76**, 224431 (2007).
[29] S. V. Isakov, M. B. Hastings, and R. G. Melko, Nat. Phys. **7**, 772 (2011).
[30] O. Derzhko, J. Richter, and M. Maksymenko, Int. J. Mod. Phys. B **29**, 1530007 (2015).
[31] C. Honerkamp, K. Wakabayashi, and M. Sigrist, EPL **50**, 368 (2000).
[32] A. C. Potter and P. A. Lee, Phys. Rev. Lett. **112**, 117002 (2014).
[33] J. S. Hofmann, F. F. Assaad, and A. P. Schnyder, Phys. Rev. B **93**, 201116(R) (2016).
[34] E. H. Lieb, Phys. Rev. Lett. **62**, 1201 (1989).
[35] M. Bercx, J. S. Hofmann, F. F. Assaad, and T. C. Lang, Phys. Rev. B **95**, 035108 (2017).
[36] H. Feldner, Z. Y. Meng, T. C. Lang, F. F. Assaad, S. Wessel, and A. Honecker, Phys. Rev. Lett. **106**, 226401 (2011).
[37] G. Z. Magda, X. Jin, I. Hagymási, P. Vancsó, Z. Osváth, P. Nemes-Incze, C. Hwang, L. P. Biró, and L. Tapasztó, Nature (London) **514**, 608 (2014).
[38] E. Tang and L. Fu, Nat. Phys. **10**, 964 (2014).
[39] R. Blankenbecler, D. J. Scalapino, and R. L. Sugar, Phys. Rev. D **24**, 2278 (1981).
[40] S. R. White, D. J. Scalapino, R. L. Sugar, E. Y. Loh, J. E. Gubernatis, and R. T. Scalettar, Phys. Rev. B **40**, 506 (1989).
[41] F. Assaad and H. Evertz, in *Computational Many-Particle Physics*, Lecture Notes in Physics, Vol. 739, edited by H. Fehske, R. Schneider, and A. Weiße (Springer, Berlin, 2008), pp. 277–356.
[42] F. F. Assaad, Phys. Rev. Lett. **83**, 796 (1999).
[43] S. Capponi and F. F. Assaad, Phys. Rev. B **63**, 155114 (2001).
[44] M. Bercx, F. Goth, J. S. Hofmann, and F. F. Assaad, SciPost Phys. **3**, 013 (2017).
[45] F. F. Assaad and I. F. Herbut, Phys. Rev. X **3**, 031010 (2013).
[46] F. Parisen Toldin, M. Hohenadler, F. F. Assaad, and I. F. Herbut, Phys. Rev. B **91**, 165108 (2015).
[47] A. W. Sandvik, Phys. Rev. B **57**, 10287 (1998).
[48] K. S. D. Beach, arXiv:cond-mat/0403055.
[49] I. Peschel, J. Stat. Mech. (2004) P06004.
[50] T. Grover, Phys. Rev. Lett. **111**, 130402 (2013).
[51] F. F. Assaad, T. C. Lang, and F. Parisen Toldin, Phys. Rev. B **89**, 125121 (2014).
[52] J. E. Drut and W. J. Porter, Phys. Rev. B **92**, 125126 (2015).
[53] J. E. Drut and W. J. Porter, Phys. Rev. E **93**, 043301 (2016).
[54] F. Parisen Toldin and F. F. Assaad, Phys. Rev. Lett. **121**, 200602 (2018).
[55] P. Broecker and S. Trebst, J. Stat. Mech. (2014) P08015.
[56] L. Wang and M. Troyer, Phys. Rev. Lett. **113**, 110401 (2014).
[57] F. F. Assaad, Phys. Rev. B **91**, 125146 (2015).
[58] P. Broecker and S. Trebst, Phys. Rev. E **94**, 063306 (2016).
[59] M. B. Hastings, I. González, A. B. Kallin, and R. G. Melko, Phys. Rev. Lett. **104**, 157201 (2010).
[60] S. Humeniuk and T. Roscilde, Phys. Rev. B **86**, 235116 (2012).

[61] J. Becker and S. Wessel, Phys. Rev. Lett. **121**, 077202 (2018).
[62] A. V. Chubukov, T. Senthil, and S. Sachdev, Phys. Rev. Lett. **72**, 2089 (1994).
[63] T. Grover and T. Senthil, Phys. Rev. B **81**, 205102 (2010).
[64] F. P. Toldin, T. Sato, and F. F. Assaad, Phys. Rev. B **99**, 155158 (2019).
[65] F. F. Assaad and T. Grover, Phys. Rev. X **6**, 041049 (2016).
[66] S. Gazit, M. Randeria, and A. Vishwanath, Nat. Phys. **13**, 484 (2017).
[67] S. Gazit, F. F. Assaad, S. Sachdev, A. Vishwanath, and C. Wang, Proc. Natl. Acad. Sci. **115**, E6987 (2018).
[68] X. Yang, S. Jiang, A. Vishwanath, and Y. Ran, Phys. Rev. B **98**, 125120 (2018).
[69] B. Swingle and T. Senthil, Phys. Rev. B **86**, 155131 (2012).
[70] H. Yao and X.-L. Qi, Phys. Rev. Lett. **105**, 080501 (2010).